Nano Research

Open Access

Research Article

Metabolically glycoengineered vesicular nanovaccine for direct antigen presentation and robust cancer immunotherapy

Xiaoyuan Fan[1,2,§], Fengxiang Liu[2,§], Xiwei Jiang[3,§], Lili Du[2], Zhonggui He[2,4], Shujun Wang[1] ✉, Jin Sun[2,4] ✉, and Kaiyuan Wang[2,4] ✉

[1] *School of Pharmacy, Shenyang Pharmaceutical University, Shenyang 110016, China*
[2] *Department of Pharmaceutics, Wuya College of Innovation, Shenyang Pharmaceutical University, Shenyang 110016, China*
[3] *School of Medical Devices, Shenyang Pharmaceutical University, Shenyang 110016, China*
[4] *Joint International Research Laboratory of Intelligent Drug Delivery Systems, Ministry of Education, Shenyang 110016, China*
[§] *Xiaoyuan Fan, Fengxiang Liu, and Xiwei Jiang contributed equally to this work.*

Cite this article: *Nano Research*, **2026**, *19*, 94908652. https://doi.org/10.26599/NR.2026.94908652

ABSTRACT: Dendritic cell (DC) vaccines have made substantial progress in cancer immunotherapy; however, their efficacy is still limited by the transient *in vivo* fate of mature DCs and suboptimal lymphatic transport. Here, we report a metabolically glycoengineered, nanovesicle-based and personalized nanovaccine (GSNVs) that displays upregulated C-C chemokine receptor 7 (CCR7) and major histocompatibility (MHC)-I complexes to promote lymph node homing and effectively presents tumor antigens to $CD8^+$ T cells, ultimately triggering a strong antigen-specific antitumor immune response. GSNVs were generated from ManNAc-engineered bone marrow-derived DCs (BMDCs) pulsed with highly immunogenic exosomes derived from senescent tumor cells. Metabolic glycoengineering endows BMDCs with enhanced antigen cross-presentation, elevated CCR7 expression, and negligible PD-L1 levels, thereby promoting robust and persistent $CD8^+$ T cell responses. Notably, GSNVs treatment elicits robust antitumor immunity, rescues T cell exhaustion, and markedly inhibits tumor growth of B16-OVA-bearing mice. Collectively, these results reveal that our metabolically glycoengineered GSNVs could be an effective strategy to overcome the inherent limitation of DC vaccines in inducing adaptive antitumor immunity for its potential application in personalized cancer immunotherapy.

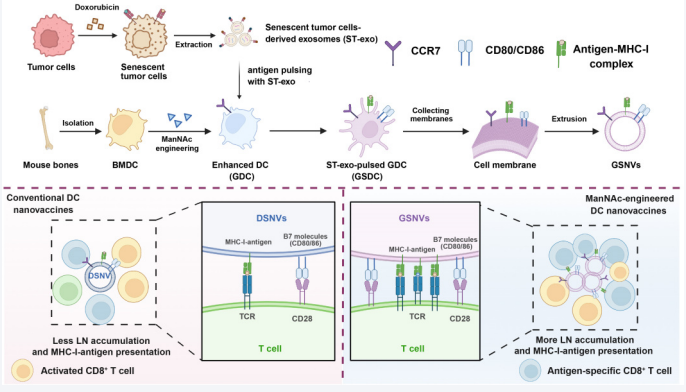

KEYWORDS: cancer immunotherapy, dendritic cell, membrane vesicles, nanovaccine, metabolic glycoengineering

1 Introduction

In recent years, immunotherapy has become a revolutionary modality in cancer treatment [1]. In contrast to the off-target effects and unsatisfactory therapeutic outcomes associated with chemotherapy and radiotherapy, immunotherapy can induce specifically potent and long-lasting antitumor effects [2]. Cancer immunotherapy leverages the host immune system to specifically recognize and eliminate cancer cells, showing remarkable potential in destroying primary tumors and reducing recurrence [3, 4]. Compared with current immunotherapeutic approaches (e.g., adoptive cell transfer, immune checkpoint blockade, and cytokine therapeutics), cancer vaccines [5, 6], particularly cell-based vaccines [7–9], represent a promising strategy capable of rapidly engaging the immune system and eliciting potent antitumor immunity. Among immune cells, dendritic cells (DCs) play an essential role in initiating and regulating adaptive immune responses [10, 11]. Due to their superior capacity to process and present tumor-associated antigens or neoantigens via major histocompatibility complex (MHC) molecules to initiate innate and adaptive immunity, DCs have been extensively used to prepare cancer vaccines as a personalized immunotherapy strategy in clinics [12–15]. The

Received: December 30, 2025; **Revised:** March 17, 2026
Accepted: March 18, 2026

✉Address correspondence to Shujun Wang, wangshujun@syphu.edu.cn; Jin Sun, sunjin@syphu.edu.cn; Kaiyuan Wang, wangkaiyuan@hotmail.com

clinical trials based on DC vaccines have successfully induced tumor-specific cytotoxic T lymphocyte (CTL) responses and even brought unexpected clinical progress [16]. However, the overall effectiveness of DC vaccines is still weak, which may mainly be attributed to the inefficient tumor-specific T cell responses induced in patients.

The first shortcoming is the weak migratory ability of *ex vivo*-generated DCs after administration [17]. Following intradermal or subcutaneous injection, only limited DCs can traffic to lymph nodes (LNs) and initiate T cell activation. Most DCs are trapped at the injection site or are cleared before reaching their immunological destinations, resulting in inefficient antigen presentation and suboptimal T cell activation [18–20]. In addition, the efficiency of antigen cross-presentation in DC vaccines is still not optimal [21], limiting their capacity to present tumor-derived antigen peptides to $CD8^+$ T cells via MHC-I molecules [22], thereby impairing the induction of robust cytotoxic T cell responses. Furthermore, a major obstacle to DC-based immunotherapy comes from the immune regulatory mechanisms that suppress vaccine efficacy. Upon adjuvant stimulation, the expression of programmed death ligand 1 (PD-L1) on DCs will be upregulated [23–25]. The PD-L1/PD-1 binding between DCs and T cells can induce T cell dysfunction, exhaustion, or even apoptosis, thereby attenuating antitumor immunity [26, 27]. Furthermore, due to the intrinsic antigenic heterogeneity among tumors [28, 29], it is often difficult to select suitable tumor antigens for *ex vivo* DC stimulation, which further leads to the suppression of the recognition efficiency and cytotoxic activity of activated T cells toward tumor cells [30]. All these obstacles result in the poor clinical effect of DC vaccines. Therefore, it is necessary to find a new strategy to enhance the trafficking of DCs to LNs, enhance the efficiency of antigen presentation by DCs, potentiate immune activation and relieve the inhibition induced by checkpoints.

With the rapid development of nanotechnology [31, 32], cell-derived nanovesicles are emerging as a promising next-generation platform for cell-based vaccination [33, 34]. DC-derived membrane vesicles harbor most of the antigen-presenting components and co-stimulatory molecules of their parent cells while showing improved stability, compatibility, and loading efficiency [35, 36]. Similar to DCs, these DC nanovesicles can migrate to LNs and present antigens to T cells with possible replacement for traditional whole-cell vaccines [37, 38]. In this work, we constructed a metabolic glycoengineering DC nanovaccine (GSNVs) to obtain enhanced antigen presentation and therapeutic effect of DC vaccines (Fig. 1). This engineering approach significantly enhanced C-C chemokine receptor type 7 (CCR7) expression on BMDCs, promoted cross-presentation of tumor antigens, and did not upregulate the immune checkpoint PD-L1. GSNVs were prepared by harvesting membrane nanovesicles from ManNAc-engineered BMDCs (GDCs) that had been pre-stimulated with senescent tumor cell-derived exosomes (ST-exo), aiming to maintain the functional integrity of their membrane proteins. The increased CCR7 expression enabled GSNVs to sense the chemokines CCL19/CCL21, thereby promoting their targeted accumulation in draining lymph nodes (dLNs) via the CCR7-CCL19/CCL21 axis. In addition, enhanced antigen cross-presentation, together with the inhibition of PD-L1 upregulation, ultimately contributes to GSNVs-mediated activation of $CD8^+$ T cells. Notably, GSNVs could elicit potent antitumor immunity, suppress the growth of B16-OVA tumors, and significantly prolong the survival of tumor-bearing mice. Meanwhile, GSNVs exhibited preferable biocompatibility and safety, indicating their potential as a clinically translatable nanovaccine platform. In this study, our nanovaccines enhanced the adaptive immune response induced by DC nanovaccines as a promising strategy for developing personalized cancer immunotherapy.

2 Experimental

2.1 Materials

N-azidoacetylmannosamine-tetraacylated (Ac_4ManNAz), DBCO-Cy3, DOX and N-acetyl-D-mannosamine (ManNAc) were obtained from Sigma-Aldrich. ELISA kits for detecting tumor necrosis factor-alpha (TNF-α), interferon-gamma (IFN-γ) and interleukin-2 (IL-2) were purchased from Invitrogen. Bicinchoninic acid (BCA) protein assay kit was purchased from Solarbio. DiD dye, radioimmunoprecipitation assay (RIPA) buffer and phenylmethylsulfonyl fluoride (PMSF) were acquired from Dalian Meilun Biotechnology Co., Ltd. (Dalian, China).

Rabbit antibodies for western blotting including anti-TSG101, anti-CD81, anti-CD9 and anti-OVA were purchased from Abcam. Fluorophore-conjugated anti-mouse antibodies for flow cytometric analysis (anti-CD11c-FITC, anti-CD80-PE, anti-CD86-APC, anti-PD-L1-PE, anti-CCR7-APC, anti-SIINFEKL-H-$2K^b$-APC, anti-SIINFEKL-H-$2K^b$-PE, anti-CD3-FITC, anti-CD8α-PerCP-Cy5.5, anti-CD4-APC, anti-CCR7-APC, anti-PD-L1-PE, anti-SIINFEKL-tetramer-PE, anti-IFN-γ-APC, anti-TIM-3-APC, and anti-PD-1-PE) were obtained from Biolegend.

2.2 Cell culture and animal model

Ovalbumin (OVA)-expressing B16F10 (B16-OVA) tumor cells were a generous gift from Professor Yongjun Wang at Shenyang Pharmaceutical University. Tumor cells were cultured in Roswell Park Memorial Institute 1640 (RPMI-1640) medium (10% fetal bovine serum (FBS), 1% Penicillin/Streptomycin) and incubated in the cell culture incubator (37 °C, 5% CO_2).

C57BL/6 mice (6–8 weeks, female) were purchased from the Laboratory Animal Center of Shenyang Pharmaceutical University. All animal experiments were performed following the guidelines approved by the Institutional Animal Care and Use Committee (IACUC) of Shenyang Pharmaceutical University. All mice were housed under specific pathogen-free (SPF) conditions in a regulated environment (temperature and humidity) and were humanely euthanized once the tumor volume exceeded 1500 mm^3.

2.3 Senescence induction

Cellular senescence was induced by treating B16-OVA cells with doxorubicin (DOX) (0, 50, 200 and 1000 nM) for 5 days [39]. After treatment, Dox-treated cells were collected and stained using an X-Gal kit (Beyotime, Shanghai) according to the manufacturer's instructions. At last, an inverted microscope (Nikon) was used to visualize senescence-associated β-galactosidase (SA-β-Gal) activity. To analyze the enhanced antigen self-presentation, senescent tumor cells were stained with anti-SIINFEKL-H-$2K^b$-APC and analyzed by flow cytometry (FACS Celesta, BD). Flow cytometry data were processed using FlowJo software (version 10.8.1).

Quantitative reverse transcription polymerase chain reaction (RT-qPCR) was performed to assess senescence-associated gene expression in normal and Dox-treated B16-OVA cells (P16, P21)

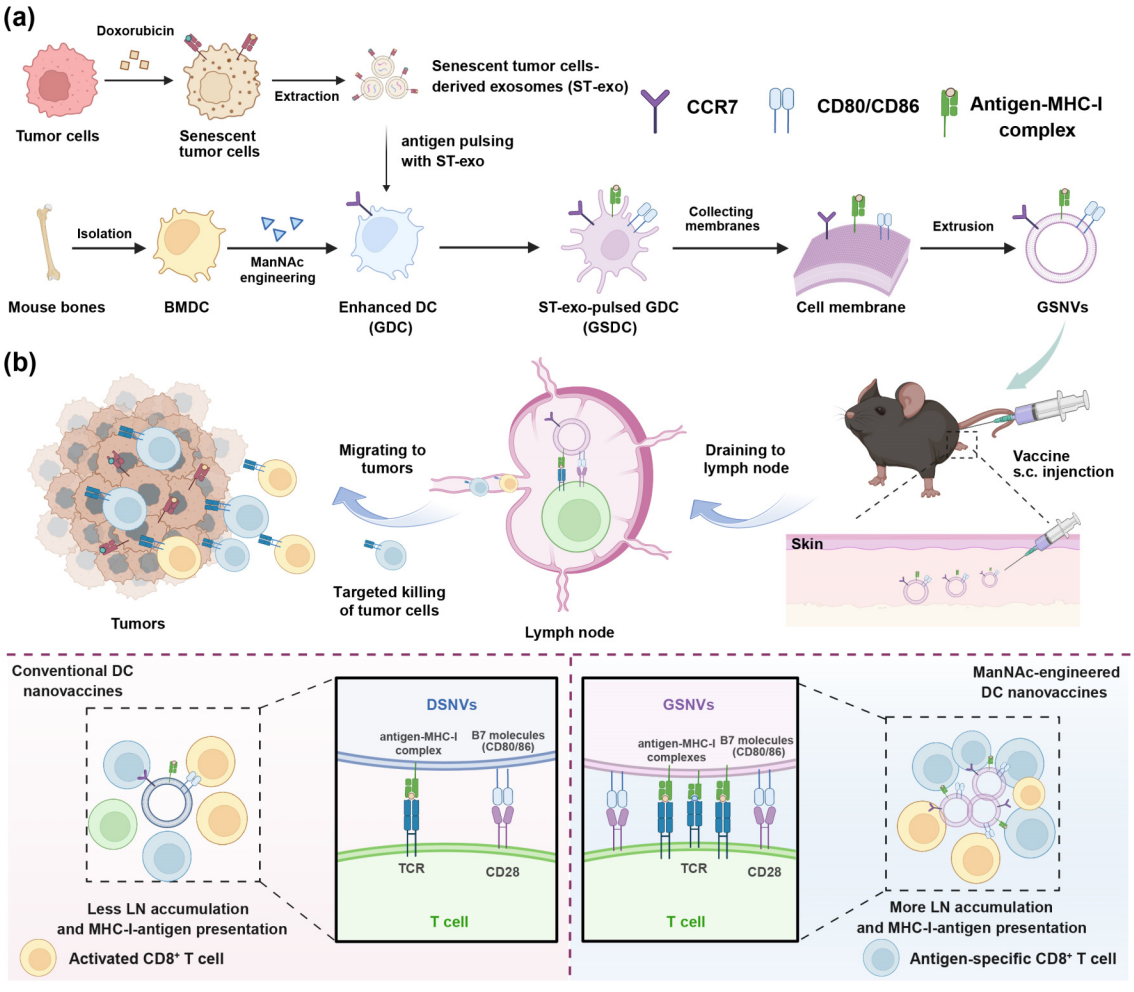

Figure 1 Schematic illustration of GSNVs acting as enhanced DC-based nanovaccines for improved cancer immunotherapy. (a) Mouse BMDCs were engineered with ManNAc and subsequently pulsed with exosomes derived from senescent B16-OVA cells. GSNVs were then fabricated from membrane nanovesicles isolated from these GSDCs. (b) GSNVs can directly present tumor antigens to $CD8^+$ T cells and elicit a potent antitumor immune response.

and pro-inflammatory gene expression in the corresponding exosomes (IFN-γ, TNF-α). Total RNA was isolated using the HiPure RNA Extraction Kit (Magen, Guangzhou). Before reverse transcription, residual genomic DNA was eliminated using gDNA wiper. First-strand complementary DNA (cDNA) was synthesized using HiScript III RT SuperMix (Vazyme, Nanjing) and quantified on a real-time PCR system (ThermoFisher). All primer sequences utilized for gene amplification are listed in Table S1 in the Electronic Supplementary Material (ESM).

2.4 Preparation and characterization of exosomes derived from senescent tumor cells

Following the induction of cellular senescence, the culture supernatants were subjected to multistep gradient centrifugation to isolate small vesicles [36]. Briefly, the supernatants were centrifuged to remove intact cells (300*g*, 5 min), followed by sequential centrifugation (3000*g*, 10 min; 8000*g*, 10 min) to remove cellular debris and larger vesicular contaminants. The supernatants were further ultracentrifuged (100,000*g*, 1 h) to collect nanosized vesicles, which were designated as ST-exo. The exosomes were then extruded through porous membranes (100 nm, Whatman), and their hydrodynamic diameter and zeta potential were determined using a Malvern Zetasizer. For control preparations, normal tumor cell-derived exosomes (T-exo) was isolated from untreated B16-OVA cells following the same protocol. The morphology of exosomes was characterized by transmission electron microscopy (TEM).

2.5 Western blotting

Proteins from Senescent B16-OVA cells (ST) and ST-exo were isolated by lysing the vesicles in RIPA buffer containing PMSF. After separation on 12% sodium dodecyl sulfate-polyacrylamide gel electrophoresis (SDS-PAGE) gels, proteins were electro-transferred onto polyvinylidene fluoride (PVDF) membranes for subsequent immunoblotting. The membranes were then immersed in blocking buffer for 2 h and exposed to primary antibodies (including anti-Ovalbumin, anti-CD63, anti-CD9, and anti-TSG101 antibodies) overnight at 4 °C. Finally, all protein bands were visualized using a Bio-Rad imaging system after incubation with a secondary antibody.

2.6 Preparation of BMDCs

To isolate BMDCs, both femurs and tibias were aseptically removed from C57BL/6 mice [40]. The cells obtained from bones were flushed into a six-well plate using cold PBS and incubated with red blood cell (RBC) lysis buffer to remove erythrocytes. Then, cells

were harvested after centrifugation (500*g*, 5 min) and cultured in a 100-mm Petri dish (1×10^6 cells/mL) containing RPMI 1640 medium (20 ng/mL of granulocyte-macrophage colony-stimulating factor (GM-CSF) and interleukin-4 (IL-4)) for BMDC differentiation. On day 7, BMDCs were harvested and used for further experiments.

2.7 Metabolic glycoengineering of BMDC

To perform metabolic glycoengineering, BMDCs were pretreated with 50 μM ManNAc for 72 h. To visualize successful engineering, Ac_4ManNAz was used as a substitute. Following incubation, engineered cells were suspended in Dulbecco's phosphate-buffered saline (DPBS) and centrifuged to remove residual Ac_4ManNAz. Subsequently, the azido groups displayed on the surface of BMDCs were fluorescently labeled with DBCO-Cy3 for 30 min. Following three washes with DPBS, Cy3-labeled BMDCs were assessed by confocal microscopy (C2SI, Nikon) and flow cytometry (FACS Celesta, BD). The levels of CCR7 and PD-L1 on BMDCs following ManNAc engineering were analyzed by staining with anti-CCR7-APC and anti-PD-L1-PE antibodies. LPS-stimulated BMDCs (LDCs) served as the control group.

2.8 Antigen presentation by DCs

BMDCs were pretreated with ManNAc or PBS (control group) for 3 days to assess the effect of metabolic glycoengineering on antigen presentation. Following pretreatment, BMDCs were pulsed with OVA protein (200 nM or 1 μM) or tumor exosomes (20 μg T-exo or ST-exo) for 24 h and collected after centrifugation. To evaluate DC maturation, cells were incubated with fluorophore-conjugated antibodies against CD80 and CD86 according to the standard procedures. The presentation of OVA-derived SIINFEKL peptide bound to MHC-I was detected using anti-SIINFEKL-H-2K^b-PE antibody by flow cytometry.

2.9 Preparation and characterization of GSNVs

To prepare cell membrane vesicles, 1×10^7 cells from each group, including ST-exo-pulsed BMDCs (SDCs), T-exo-pulsed GDCs (GTDCs), ST-exo-pulsed GDCs (GSDCs), and ST-exo-pulsed LDCs (LSDCs), were resuspended in sterile saline containing protease inhibitor and subjected to sonication at 20 W for 5 min. The lysates were then clarified through sequential centrifugation (2000, 5000 and 15,000 r/min) to remove whole cells and cellular debris. The resulting membrane fragments were resuspended in 1 mL of deionized water and serially extruded through polycarbonate membranes of decreasing pore sizes (400, 200 and 100 nm) utilizing an Avanti Mini-Extruder. The final nanovesicles were collected by centrifugation and stored at 4 °C. The nanovesicles derived from SDCs, GTDCs, GSDCs, and LSDCs were designated as DSNVs, GTNVs, GSNVs, and LSNVs, respectively. Their particle size and morphology were characterized using a Malvern Zetasizer and TEM (Hitachi).

2.10 Pull down assay

All prepared vesicular nanovaccines were first incubated with 1% bovine serum albumin (BSA) (5 mg/mL) to minimize nonspecific adsorption to the vesicle surface. Subsequently, all nanovesicles were incubated with anti-CD80, anti-CD86, anti-SIINFEKL-H-2K^b, anti-CCR7 or anti-PD-L1 fluorophore-conjugated antibodies for 30 min. Following ultracentrifugation of the mixed samples to pellet the exosomes, the measurement of supernatant fluorescence intensity was carried out using a Multifunctional microplate reader (ThermoFisher). Antibody binding efficiency was assessed based on the reduction in fluorescence intensity between the original antibody solution and the post-centrifugation supernatant.

2.11 Preparation of T cells

To isolate T cells, a C57BL/6 mouse was euthanized, and the spleen was aseptically removed. After rinsing with cold PBS, the mouse spleen was gently homogenized to prepare splenocyte suspensions. Following erythrocyte lysis, the cell suspension was quenched with 3 mL of PBS to halt further lysis. Splenocytes were obtained following centrifugation and resuspended in 2 mL of PBS, and CD3$^+$ T cells were purified using the Beaver Mouse CD3 T Cell Isolation Kit.

2.12 *In vitro* CD8$^+$ T cell activation

To evaluate the GSNVs-mediated direct CD8$^+$ T cell activation, isolated mouse T cells were pre-incubated using anti-CD3 and anti-CD28 antibodies, and incubated with PBS, DSNVs, GTNVs and GSNVs for 3 days. Following treatment, T cells were pretreated with an anti-CD16/32 antibody for Fc receptor blocking and stained with anti-CD8*α*-PerCP-Cy5.5 for flow cytometric analysis. Cytokine secretion (TNF-*α* and IFN-*γ*) from activated T cells was assessed via enzyme-linked immunosorbent assay (ELISA) according to the manufacturer's guidelines.

2.13 Migration of GSNVs to LNs

To investigate the LN trafficking capability of GSNVs, C57BL/6 mice received subcutaneous injections of DiD dye, DiD-labeled DSNVs or DiD-labeled GSNVs (20 μg DiD per mouse) at the tail base. Twenty-four hours post-injection, the dLNs were excised and subjected to *ex vivo* fluorescence imaging using the IVIS system (PerkinElmer). In addtion, the dLNs were cryo-sectioned into 10-μm-thick slices and stained with 4',6-diamidino-2-phenylindole (DAPI) for 5 min. After thorough washing, tissue slices were subsequently imaged to visualize the LN accumulation of nanovaccines with a confocal microscope.

2.14 *In vivo* immunization and biosafe assessment

Briefly, C57BL/6 mice were subcutaneously vaccinated with PBS, DSNVs, GTNVs, and GSNVs (100 μg nanovesicles per mouse) for three consecutive immunizations on days 0, 3 and 6. Four days following the final immunization, splenocytes were obtained by mechanically grinding spleens harvested from vaccinated mice and then resuspended in staining buffer. After anti-CD16/32 antibody (Biolegend) blocking, cells were incubated with anti-CD3, anti-CD8*α*, and anti-SIINFEKL-tetramer fluorophore-conjugated antibodies to specifically stain OVA-specific CD8$^+$ T cells. Assessment of T cell responses was performed by re-stimulating splenocytes with nanovesicle lysates. The secretion of IL-2, IFN-γ and TNF-*α* by activated immune cells was measured via ELISA. To evaluate the *in vivo* safety profile of GSNVs, female C57BL/6 mice were monitored following vaccination. Seven days after receiving the final vaccination, blood samples were collected via retro-orbital blood collection for serum biochemical analyses, including liver and kidney function markers (alanine aminotransferase (ALT), aspartate aminotransferase (AST), blood urea nitrogen (BUN) and creatinine (CREA)). To assess possible tissue toxicity, major organs from GSNVs-treated mice were harvested and examined by hematoxylin and eosin (H&E) staining.

2.15 Immune exhaustion assessment

To assess potential adverse effects, such as immune exhaustion, induced by GSNVs administration, C57BL/6 mice were subcutaneously administered with PBS, DSNVs, LSNVs and GSNVs on days 0, 3 and 6. Four days post-final immunization, spleens were harvested to evaluate the expression of immune exhaustion markers. Spleens were mechanically dissociated to generate single-cell suspensions. The obtained splenocytes were blocked with anti-CD16/32 antibody and subsequently stained with a panel of fluorophore-conjugated antibodies, including anti-CD3-FITC, anti-CD8α-PerCP-Cy5.5 and anti-LAG3-PE, followed by analysis with flow cytometry.

2.16 *In vivo* cancer immunotherapy of GSNVs

For the therapeutic evaluation, 5×10^5 B16-OVA cells were subcutaneously injected into the right flank of C57BL/6 mice to establish tumor-bearing models. Following tumor inoculation, randomly assigned mice were treated with PBS, DSNVs, GTNVs, or GSNVs on days 6, 9 and 12, with each mouse receiving 100 μg of nanovesicles per administration. To evaluate tumor progression and animal health, tumor volumes (V = length × width^2/2) and body weights were recorded every 3 days throughout the study.

Seven days after treatment completion, tumors were harvested from vaccinated mice and ground in medium (1 mg/mL collagenase IV and 0.2 mg/mL deoxyribonuclease I (DNase I)) for immunological assays via flow cytometry. Subsequently, single-cell suspensions generated from tumor tissues were subjected to anti-CD16/32 antibody blocking and stained with a panel of fluorophore-conjugated antibodies, including anti-CD45, anti-CD3, anti-CD8α, anti-SIINFEKL tetramer and anti-IFN-γ antibodies. The enhanced infiltration of CD8$^+$ T cells within tumor tissues was visualized via immunofluorescence image analysis. Briefly, sections from tumor tissues were prepared in paraffin and subjected to immunofluorescence staining using an anti-CD8-FITC antibody. Additionally, supernatants from these tumor cell suspensions were collected to determine TNF-α and IFN-γ levels by ELISA.

To demonstrate the advantage of metabolic glycoengineering, we compared the antitumor efficacy of GSNVs and LSNVs. Briefly, mice bearing subcutaneous B16-OVA tumors were established and vaccinated with PBS, LSNVs, or GSNVs on days 6, 9, and 12 after tumor inoculation. Each mouse received 100 μg of nanovesicles per injection via subcutaneous administration. Tumor volumes were recorded every 3 days throughout the study. On day 21 after tumor inoculation, tumors were harvested from vaccinated mice and processed into single-cell suspensions. Cells were stained with fluorophore-conjugated antibodies against CD45, CD3, CD8α, T cell immunoglobulin and mucin domain-containing protein 3 (TIM-3), and PD-1, followed by flow cytometric analysis.

2.17 Statistical analysis

Data were expressed as mean ± standard deviation (SD) in this study. Data analyses were performed using GraphPad Prism 9. Unpaired two-tailed Student's t-test was applied for comparisons between two groups. Statistical significance among multiple groups was analyzed by one-way ANOVA with Dunnett's or Tukey's comparison. Survival curves were compared using the log-rank (Mantel-Cox) test. P value less than 0.05 was considered statistically significant, $^*P < 0.05$, $^{**}P < 0.01$, $^{***}P < 0.001$, $^{****}P < 0.0001$.

3 Results and discussion

3.1 Characterization of senescent tumor exosomes

In addition to immunoadjuvants, the selection of appropriate tumor antigens plays a pivotal role in determining vaccine efficacy. However, the intrinsic antigenic heterogeneity among tumors often results in suboptimal therapeutic outcomes. To address this limitation, whole tumor cells or tumor cell-derived vesicles have been employed to pulse DC vaccines [41, 42], thereby enhancing T cell recognition and promoting subsequent tumor cell elimination. Notably, the immunogenicity of tumor cells is profoundly influenced by their physiological state. In particular, senescent tumor cells typically exhibit elevated antigen-MHC-I complexes on the cell surface, thereby facilitating CD8$^+$ T cell-mediated tumor destruction [43]. Owing to their enhanced immunogenicity, senescent tumor cells have emerged as valuable antigen reservoirs that can elicit strong immune responses. To generate senescent models, B16-OVA cells were exposed to various concentrations of DOX for 5 days and subsequently examined with a SA-β-Gal staining kit (Fig. 2(a)). When treated with 200 nM DOX, over 80% of cells were positive for SA-β-Gal staining (Figs. 2(b) and 2(c)). Because a higher concentration (1000 nM) caused evident cytotoxicity, 200 nM was chosen as the optimal dose to induce senescence in B16-OVA cells (Fig. 2(b)). Morphologically, DOX-treated cells exhibited enlarged, flattened shapes characteristic of senescence. Moreover, DOX-induced senescence markedly enhanced the expression of SIINFEKL-H-2K^b complexes (Fig. 2(d) and Fig. S1 in the ESM), suggesting improved immunogenicity of B16-OVA melanoma cells. In addition, proinflammatory cytokines (IFN-γ and IL-6) and senescence-related mRNA levels (P16 and P21) were substantially upregulated (Figs. 2(e)–2(h)). Collectively, these findings suggest that DOX treatment efficiently induced B16-OVA cells towards a stable senescent state.

The resulting senescent tumor cell-derived vesicles, enriched with tumor-associated antigens and nucleic acids, effectively activate DCs, underscoring their potential as promising platforms for nanovaccine construction [44]. Exosomes were subsequently purified from the supernatants of normal (T-exo) and senescent (ST-exo) B16-OVA cells through differential centrifugation. TEM analysis showed that both T-exo and ST-exo possessed the typical cup-shaped morphology of exosomes, with an average diameter of approximately 120 nm and a uniform size distribution (Figs. 2(i) and 2(j)). Compared with the whole senescent cells, the presence of exosome markers, including TSG101, CD63, and CD9 proteins, was detected in ST-exo (Fig. 2(k)). To evaluate their immunostimulatory properties, the gene levels of immune-related cytokines were measured. RT-qPCR analysis showed that the mRNA levels of IFN-γ and TNF-α were significantly upregulated in ST-exo (Fig. 2(l)). Overall, these results indicate that senescent tumor cells showed increased immunogenicity, and their senescent exosomes inherited this advantage. The resulting vesicles derived from senescent tumor cells are enriched in tumor-associated antigens and nucleic acids, making them a promising antigen reservoir for constructing enhanced nanovaccines.

3.2 Enhanced antigen-presenting activity of GDCs

To verify the successful metabolic glycoengineering, BMDCs were treated with 50 μM $Ac_4ManNAz$, a synthetic ManNAc analogue, to introduce azide ($-N_3$) groups into the cell membrane. After 72 h of treatment, cells were labeled with DBCO-Cy3 for visualization. In

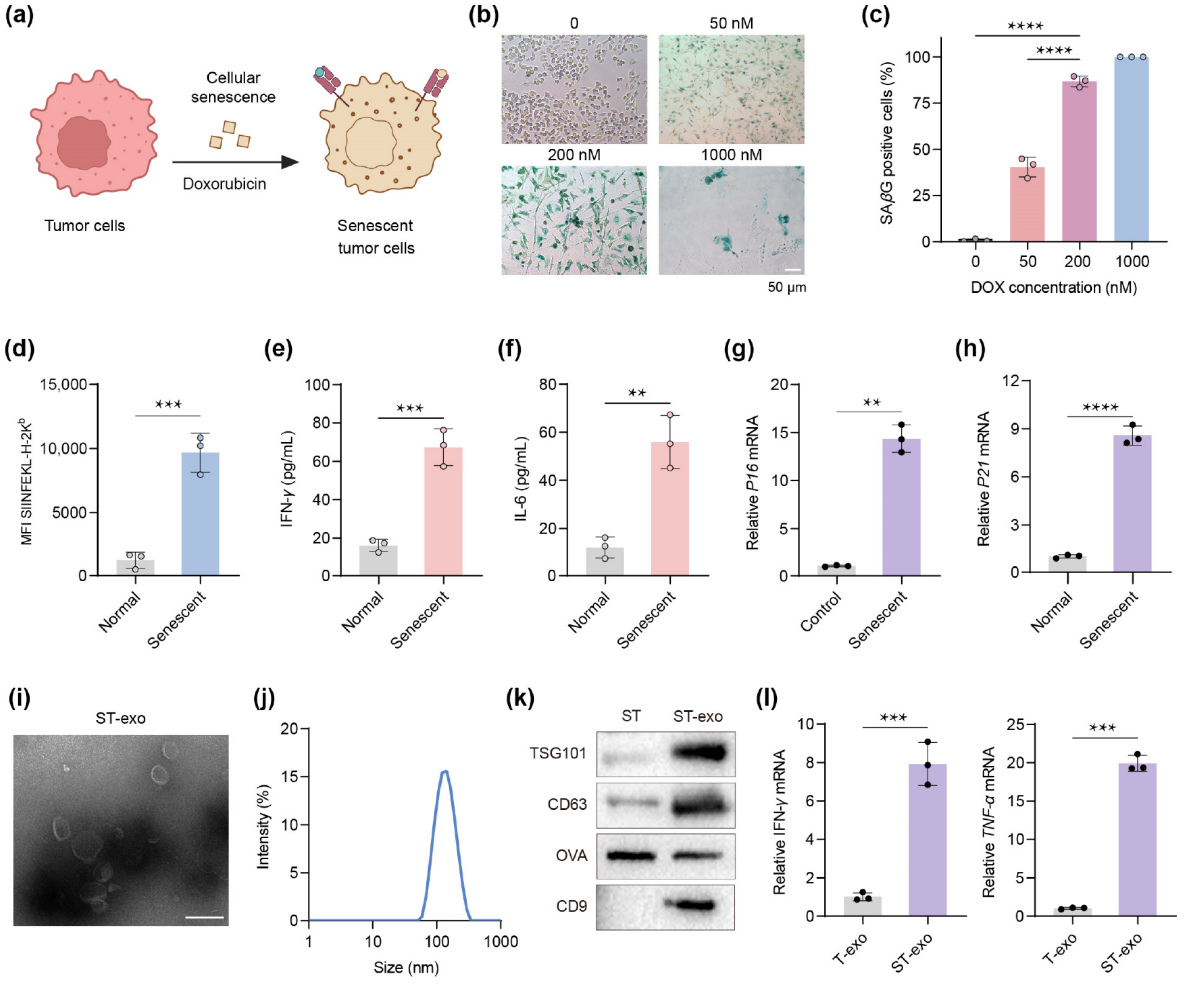

Figure 2 Preparation and characterization of senescent B16-OVA exosomes. (a) Schematic illustration of the induction of cellular senescence. (b) Representative images of SA-β-Gal staining in B16-OVA cells treated with different concentrations (0, 50, 200, 1000 nM) of senescence-inducing agent. Scale bar: 50 μm. (c) Quantification of SA-β-Gal positive cells under different treatment conditions (n = 3). (d) Flow cytometric analysis of SIINFEKL-H-2K^b complex expression on normal and senescent B16-OVA cells (n = 3). ELISA quantification of cytokine secretion ((e) IFN-γ and (f) IL-6) from normal and senescent tumor cells (n = 3). Relative mRNA expression levels of senescence markers (g) P16 and (h) P21 in normal and senescent cells (n = 3). (i) TEM image of ST-exo showing typical exosomal morphology. Scale bar: 200 nm. (j) Size distribution of ST-exo measured by a Malvern Zetasizer. (k) Western blotting analysis of exosomal markers (TSG101, CD63, CD9) and OVA in ST and ST-exo. (l) Relative mRNA expression levels of inflammatory cytokines (IFN-γ and TNF-α) in T-exo and ST-exo (n = 3). Data were expressed as mean ± SD. $^{**}P < 0.01$, $^{***}P < 0.001$, $^{****}P < 0.0001$.

Ac_4ManNAz-treated BMDCs, a strong Cy3 fluorescence signal was distributed along the cell membrane of BMDCs, whereas negligible fluorescence signal was detected in the untreated control group (Fig. 3(a)), confirming the successful incorporation of azido groups. Flow cytometric analysis further confirmed that more than 75% of engineered BMDCs were Cy3-positive (Fig. 3(b) and Fig. S2 in the ESM). Interestingly, ManNAc-engineered DCs showed a significant increase in CCR7 expression, indicating enhanced LN targeting ability (Fig. 3(c) and Fig. S3 in the ESM). In most current DC vaccines, DCs need to be pre-stimulated with immune agonists, such as LPS, to upregulate the expression of co-stimulatory molecules and thereby improve vaccine efficacy [24]. However, this process is usually accompanied by an undesirable upregulation of PD-L1, which suppresses T-cell responses. In contrast, ManNAc-treated BMDCs maintained lower expression of PD-L1 (Fig. 3(d) and Fig. S4 in the ESM), indicating that this engineering strategy may avoid such immunosuppressive effects.

To explore whether metabolic glycoengineering could improve the processing and presentation of tumor antigens by DCs, we first pulsed GDCs with OVA protein at different concentrations (200 nM and 1 μM). Under these two conditions, GDCs showed increased expression of SIINFEKL-MHC-I complexes compared to untreated DCs [45] (Figs. 3(e) and 3(f), and Fig. S5 in the ESM). The ability of MHC-I molecules to present tumor antigens is essential for initiating the activation of tumor-specific CD8$^+$ T cells and eliciting long-lasting antitumor immune responses. Next, we investigated whether ManNAc engineering could also enhance the cross-presentation of tumor exosome-derived antigens. To this end, BMDCs were incubated with T-exo or ST-exo and then analyzed by flow cytometry. Compared with normal BMDCs, GDCs showed significantly increased presentation of tumor-associated antigens, as evidenced by the increased SIINFEKL-MHC-I complexes on GDCs with T-exo or ST-exo stimulation (Figs. 3(g) and 3(h), and Fig. S6 in the ESM), indicating that ManNAc engineering endows BMDCs with a stronger ability to process and present tumor antigens. Due to the increased immunogenicity of senescent exosomes, GDCs treated with ST-exo exhibited enhanced MHC-I-restricted antigen presentation compared to those exposed to T-exo. To further assess

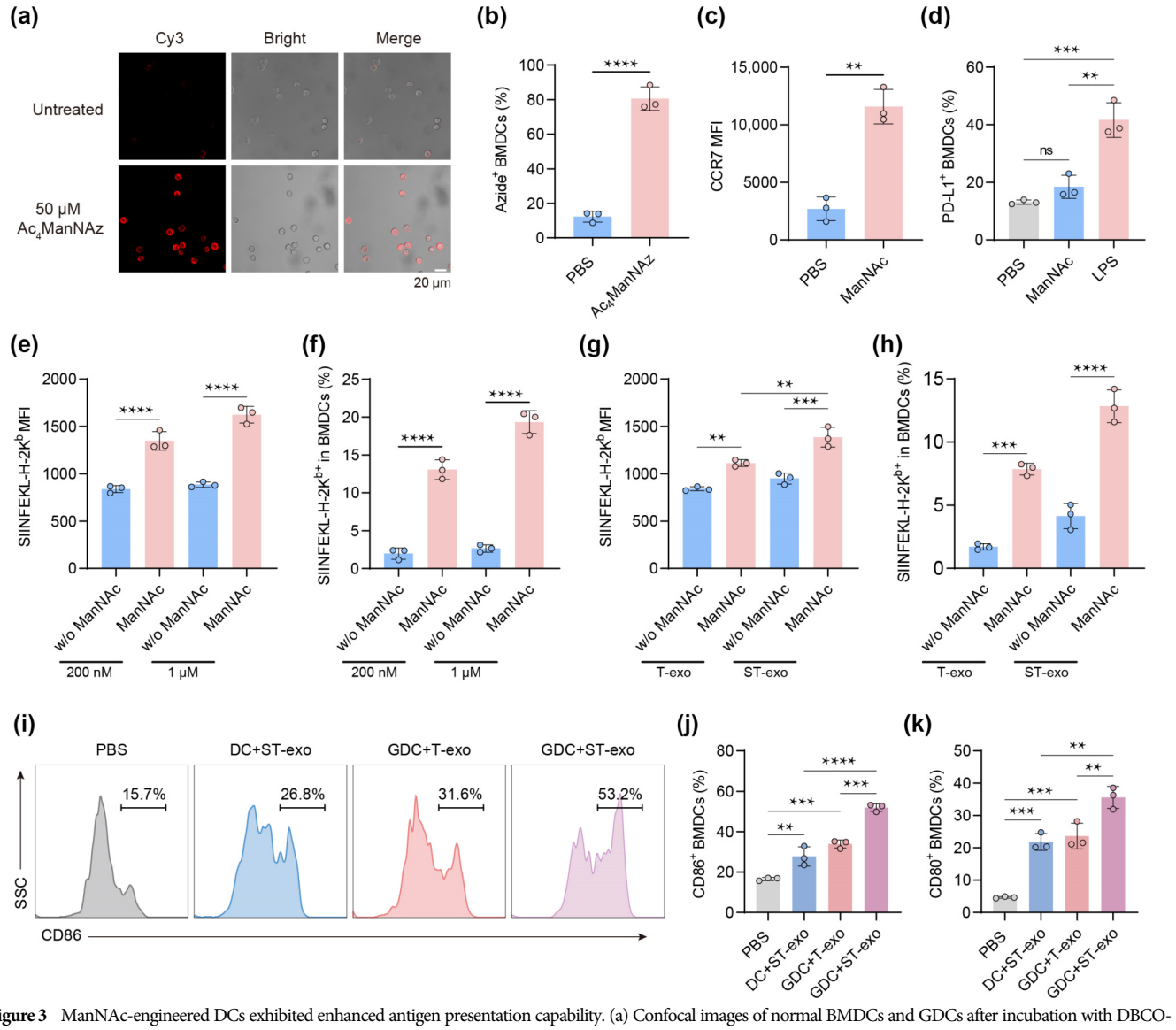

Figure 3 ManNAc-engineered DCs exhibited enhanced antigen presentation capability. (a) Confocal images of normal BMDCs and GDCs after incubation with DBCO-Cy3. Scale bar: 20 μm. (b) Percentages of azide$^+$ BMDCs following DBCO-Cy3 treatment (n = 3). (c) Mean fluorescence intensity (MFI) of CCR7 on BMDCs with or without ManNAc treatment (n = 3). (d) MFI of PD-L1 on BMDCs treated with PBS, LPS or ManNAc (n = 3). (e) MFI and (f) percentages of the SIINFEKL-H-2K^b positive BMDCs, DCs were pulsed with OVA (200 nM or 1 μM) (n = 3). (g) MFI and (h) percentages of the SIINFEKL-H-2K^b positive BMDCs, DCs were incubated with 20 μg T-exo or ST-exo (n = 3). (i) Representative flow cytometric histograms and (j) quantitative analysis of CD86 expression on BMDCs treated with PBS or ST-exo, and on GDCs pulsed with T-exo or ST-exo (n = 3). (k) Quantitative analysis of the percentages of CD80$^+$ BMDCs in various groups (n = 3). Data were expressed as mean ± SD. $^{**}P < 0.01$, $^{***}P < 0.001$, $^{****}P < 0.0001$.

DC maturation, GDCs were pulsed with T-exo or ST-exo, and the expression levels of co-stimulatory molecules were measured via flow cytometry. The results showed a significant increase in the percentages of CD80$^+$ and CD86$^+$ BMDCs when GDCs were pulsed with ST-exo (Figs. 3(i)–3(k) and Fig. S7 in the ESM). Overall, these findings indicate that the combination of ManNAc engineering and ST-exo stimulation could enhance BMDC maturation and antigen cross-presentation, potentially boosting CD8$^+$ T cell responses induced by DC vaccines.

3.3 Construction and characterization of GSNVs

Although DC-based whole-cell vaccines are capable of inducing antigen-specific immune responses, they bear several inherent weaknesses, including poor stability during *in vitro* processing and short-lived *in vivo* persistence. These shortcomings significantly impede their clinical translation [19]. To address these obstacles, we developed a DC-based nanovaccine, which maintains the antigen-presenting and co-stimulatory functions of the original cells and offers improved structural and storage stability. This nanovaccine, termed GSNVs, was fabricated by subjecting ST-exo-pulsed GDCs to sonication, followed by multistep gradient ultracentrifugation and sequential extrusion through membranes of decreasing pore size (Fig. 4(a)). DSNVs were generated with normal BMDCs pre-stimulated with ST-exo and used as a negative control. TEM images revealed that both DSNVs and GSNVs exhibited typical spherical morphologies with lipid bilayer structures (Fig. 4(b)), which demonstrated that ManNAc engineering did not cause damage to the membrane structure. These two nanovaccines had narrow size distributions with an average hydrodynamic diameter of ~ 120 nm (Fig. 4(c)), which is conducive to LN accumulation and DC

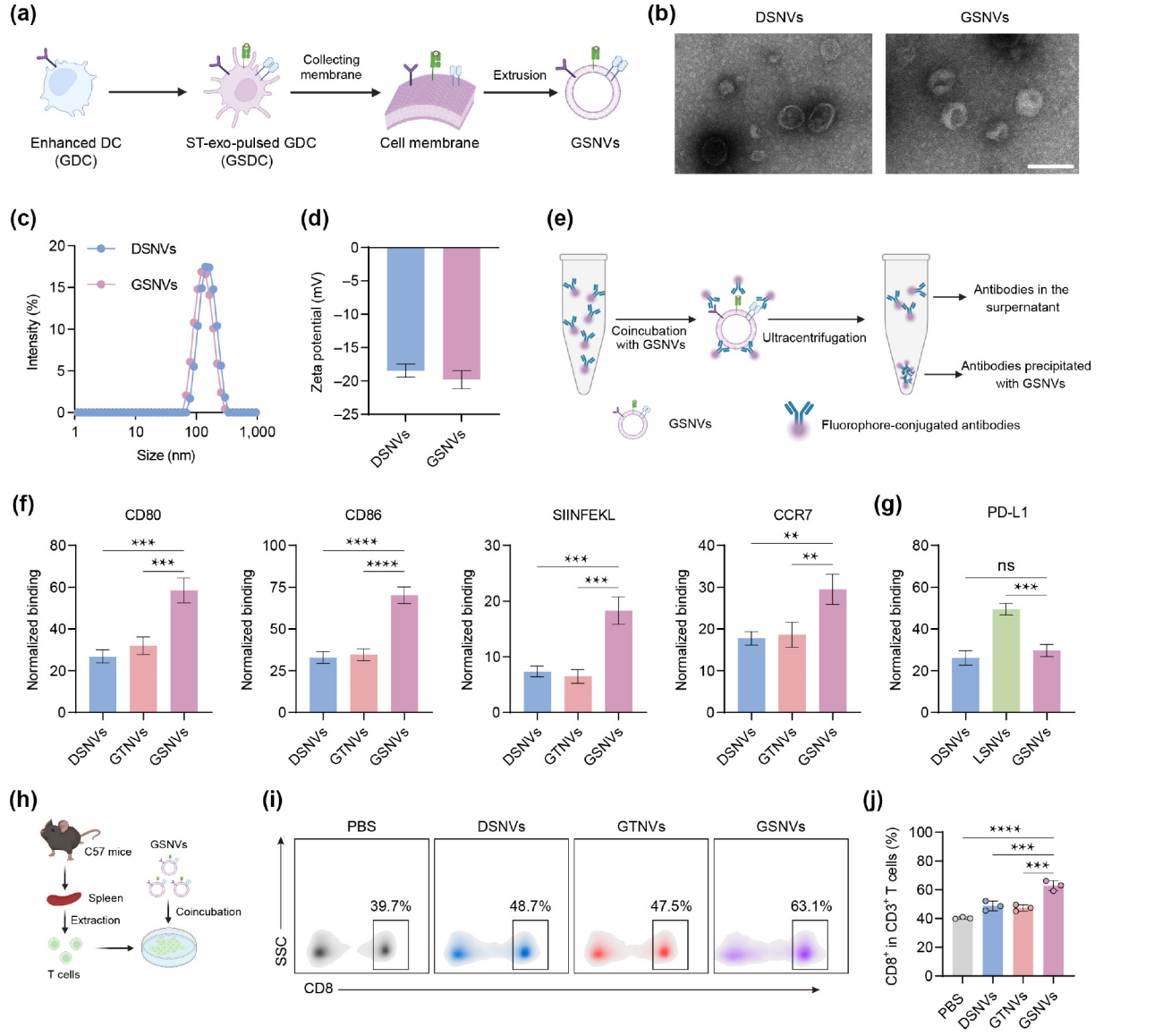

Figure 4 Preparation and characterization of GSNVs. (a) Schematic illustration of the construction of GSNVs. (b) TEM images of DSNVs and GSNVs. Scale bar: 200 nm. (c) Particle size distribution and (d) zeta potential of DSNVs and GSNVs. (e) Visualization of the design of the pull-down assay. Fluorophore-conjugated antibodies targeting CD80, CD86, CCR7, PD-L1 or SIINFEKL-H-2K^b were incubated with nanovesicles, and unbound antibodies were removed by ultracentrifugation. (f) Quantitative analysis of normalized binding of CD80, CD86, SIINFEKL-H-2K^b or CCR7 on various nanovesicles (n = 3). (g) Quantitative analysis of normalized binding of PD-L1 on various nanovesicles (n = 3). (h) Schematic illustration of the study design of *in vitro* T cell activation mediated by GSNVs. (i) Representative flow cytometric plots and (j) quantitative analysis showing CD8$^+$ T cell proliferation induced by different DC nanovaccines (n = 3). Data are presented as mean ± SD. $^{**}P < 0.01$, $^{***}P < 0.001$, $^{****}P < 0.0001$.

internalization *in vivo*. The stability of GSNVs was further evaluated after storage in saline at 4 °C. The average size of GSNVs showed no significant change for 1 week (Fig. S8 in the ESM). In addition, GSNVs and DSNVs exhibited zeta potential of about −20 and −18 mV, respectively (Fig. 4(d)). The similar characteristics between GSNVs and DSNVs indicate that ManNAc engineering mainly affects the immunomodulatory function of nanovaccines, rather than their structural or physical properties. Overall, the nanoscale properties of GSNVs contribute to effective lymphatic transport, LN accumulation, and subsequent T cell activation.

To assess whether GSNVs retain the key functional membrane proteins of their parental cells, we conducted a fluorescence-based pull-down assay [41]. As shown in Fig. 4(e), GSNVs were incubated with fluorophore-labeled antibodies targeting key immune-related surface molecules, including CD80, CD86, SIINFEKL-H-2K^b, CCR7 and PD-L1. GTNVs and LSNVs were prepared as control groups (Fig. S9 in the ESM). Notably, when incubated with antibodies that recognize CD80, CD86, and SIINFEKL-MHC-I complexes, GSNVs showed the strongest fluorescence intensity (Fig. 4(f)), indicating the preservation of T cell activation-related molecules and antigen presentation capability from the parental GDCs. In contrast, the fluorescence binding of DSNVs was weaker. In addition, significant anti-CCR7 antibody binding was detected on GSNVs, confirming successful maintenance of CCR7 on the vesicle surface (Fig. 4(f)). The high levels of CCR7 expression is particularly important for efficient lymphatic trafficking and initiation of adaptive immune responses *in vivo* [46, 47]. Compared with LSNVs, GSNVs showed lower binding to anti-PD-L1 antibody

(Fig. 4(g)), suggesting a minimal risk of triggering T cell exhaustion during activation. Collectively, these results indicate that GSNVs inherit essential functional membrane proteins from parental GDCs, including co-stimulatory molecules (CD80/CD86) and antigen-MHC-I complexes, while preserving upregulated CCR7 and low PD-L1 levels required for targeted LN delivery and robust T cell activation. Additionally, T cells were isolated from the spleens of the immunized mice and co-cultured with different nanovaccines to evaluate the ability of GSNVs to directly stimulate $CD8^+$ T cells *ex vivo* (Fig. 4(h)). As demonstrated in Figs. 4(i) and 4(j), GSNVs treatment markedly enhanced $CD8^+$ T cell expansion compared with the other control groups. Moreover, in the GSNVs group, the highest IFN-γ and TNF-α secretion was detected (Fig. S10 in the ESM), both of which are crucial for cytotoxic T cell effector functions. Collectively, these results suggest that GSNVs could directly activate and expand $CD8^+$ T cells *ex vivo*, ultimately contributing to enhanced antitumor immunity

3.4 Lymph node accumulation and potent antitumor immune responses induced by GSNVs

To examine whether GSNVs exhibit enhanced lymphatic trafficking, we first analyzed their biodistribution *in vivo* following subcutaneous administration. As illustrated in Fig. 5(a), the schematic outlines how nanovaccines traffic to the dLNs after subcutaneous injection. Twenty-four hours post-injection, IVIS imaging revealed markedly stronger fluorescence signals in the inguinal LNs of GSNVs-treated mice compared with those receiving DSNVs or free DiD dye (Fig. 5(b)). Quantitative analysis of fluorescence intensity further confirmed the enhanced LN accumulation of GSNVs (Fig. 5(c)), suggesting their superior LN-targeting ability. Consistently, fluorescence microscopy of LN sections showed a broader and more intense DiD distribution in the GSNVs group (Fig. 5(d)), indicating more efficient entry and retention within the LN tissues. Together, these observations demonstrated that GSNVs preferentially accumulated in LNs after administration, likely attributable to the preserved CCR7 expression on their surface. To further evaluate the immunostimulatory efficacy of GSNVs *in vivo*, mice were immunized with PBS, DSNVs, GTNVs, and GSNVs according to the schedule illustrated in Fig. 5(e), and mouse splenocytes were collected 4 days post-final immunization for cytokine evaluation. As shown in Figs. 5(f)–5(h), splenocytes isolated from GSNVs-vaccinated mice produced significantly higher levels of IL-2, IFN-γ and TNF-α upon re-stimulation with tumor antigens compared with those from the DSNVs and GTNVs groups. These findings indicate that GSNVs induced a robust systemic immune response.

We next analyzed the splenic OVA-specific $CD8^+$ T cells on day 10. Flow cytometric analysis revealed that mice immunized with GSNVs exhibited the highest proportion of SIINFEKL-tetramer-positive $CD8^+$ T cells compared with the PBS, DSNVs, or GTNVs groups (Figs. 5(i) and 5(j)). The increase in antigen-specific cytotoxic T cells demonstrated that GSNVs could present tumor antigens to $CD8^+$ T cells, surpassing the efficiency of conventional DC nanovaccines. In addition to antigen-specific activation, we also evaluated T cell exhaustion by examining the expression of the inhibitory receptor lymphocyte activation gene 3 (LAG3) using flow cytometry [47]. We then prepared LSNVs as a control group. Vaccination with GSNVs significantly reduced the LAG-3 expression on splenic $CD8^+$ T cells compared with LSNVs-treated group (Figs. 5(k) and 5(l)). The reduced proportion of $LAG3^+CD8^+$ T cells indicates that GSNVs not only stimulate strong antigen-specific responses but also mitigate T cell dysfunction during immune activation [48]. Collectively, these results demonstrate that GSNVs could efficiently traffic to mouse LNs, elicit robust antigen-specific antitumor T cell responses, and alleviate immune exhaustion. Moreover, the analysis of serum biochemistry indicated that GSNVs vaccination did not cause any abnormalities in the serum levels of ALT, AST, BUN and CREA (Fig. S11 in the ESM), demonstrating the good safety of GSNVs [49]. In addition, H&E staining revealed no obvious tissue damage in mice treated with GSNVs (Fig. S12 in the ESM).

3.5 Antitumor effects of GSNVs *in vivo*

We then assessed the antitumor effect of GSNVs in C57BL/6 mice bearing subcutaneous B16-OVA tumors (Fig. 6(a)). Tumor-bearing mice received various treatments, including PBS, DSNVs, GTNVs, and GSNVs. Compared with the PBS and other treatment groups, GSNVs vaccination led to a pronounced suppression of tumor growth (Fig. 6(b) and Fig. S13 in the ESM). Tumor growth in GSNVs-treated mice was significantly inhibited throughout the study, with tumor volumes reduced by more than 50% on day 24 compared with the DSNVs-treated group. Notably, more than 80% of mice immunized with GSNVs survived beyond 35 days, whereas all animals in the control groups succumbed by day 36 (Fig. 6(c)).

To characterize the underlying immune mechanisms responsible for tumor inhibition, we employed flow cytometric analysis to analyze the phenotypes of tumor-infiltrating $CD8^+$ T cells. Compared with other treatments, GSNVs treatment significantly enhanced tumor infiltration of IFN-γ^+CD8^+ T cells, suggesting that a large number of cytotoxic T cells were involved in the antitumor immune response (Figs. 6(d) and 6(e)). In addition, the mice injected with GSNVs displayed a considerable enrichment of SIINFEKL-specific $CD8^+$ T cells in the tumor tissues, demonstrating that the antigen-specific antitumor immunity was effectively activated (Figs. 6(f) and 6(g)). In contrast, DSNVs and GTNVs treatments led to a slight accumulation of $CD8^+$ CTLs in tumor tissues. Meanwhile, the immunofluorescence imaging also demonstrated that $CD8^+$ T cells widely existed in tumor sections of GSNVs-treated mice (Fig. 6(h)), further confirming GSNVs could stimulate T cell-mediated antitumor responses in B16-OVA-bearing mice. Notably, no significant changes in body weight were observed in GSNVs-treated mice (Fig. S14 in the ESM), supporting that the GSNVs nanovaccine possessed good biosafety performance. In addition, the TNF-α and IFN-γ levels were further evaluated in the tumor tissues to assess immune activation. The results indicate that the mice injected with GSNVs exhibited markedly higher concentrations of TNF-α and IFN-γ compared with the control groups (Figs. 6(i) and 6(j)), which contributed to enhanced effector T cell activity and finally led to improved antitumor efficacy [50]. Collectively, our results demonstrate that GSNVs induce potent and durable antitumor immunity in B16-OVA-bearing mice, as evidenced by increased tumor infiltration of IFN-γ^+ and SIINFEKL-specific $CD8^+$ T cells and enhanced TNF-α and IFN-γ production by tumor-infiltrating T lymphocytes.

To further compare the efficacy of ManNAc-engineered and LPS-stimulated DC nanovaccines, B16-OVA tumor-bearing mice were vaccinated with GSNVs or LSNVs. As shown in Fig. S15 in the ESM, LSNVs suppressed tumor growth, but their antitumor

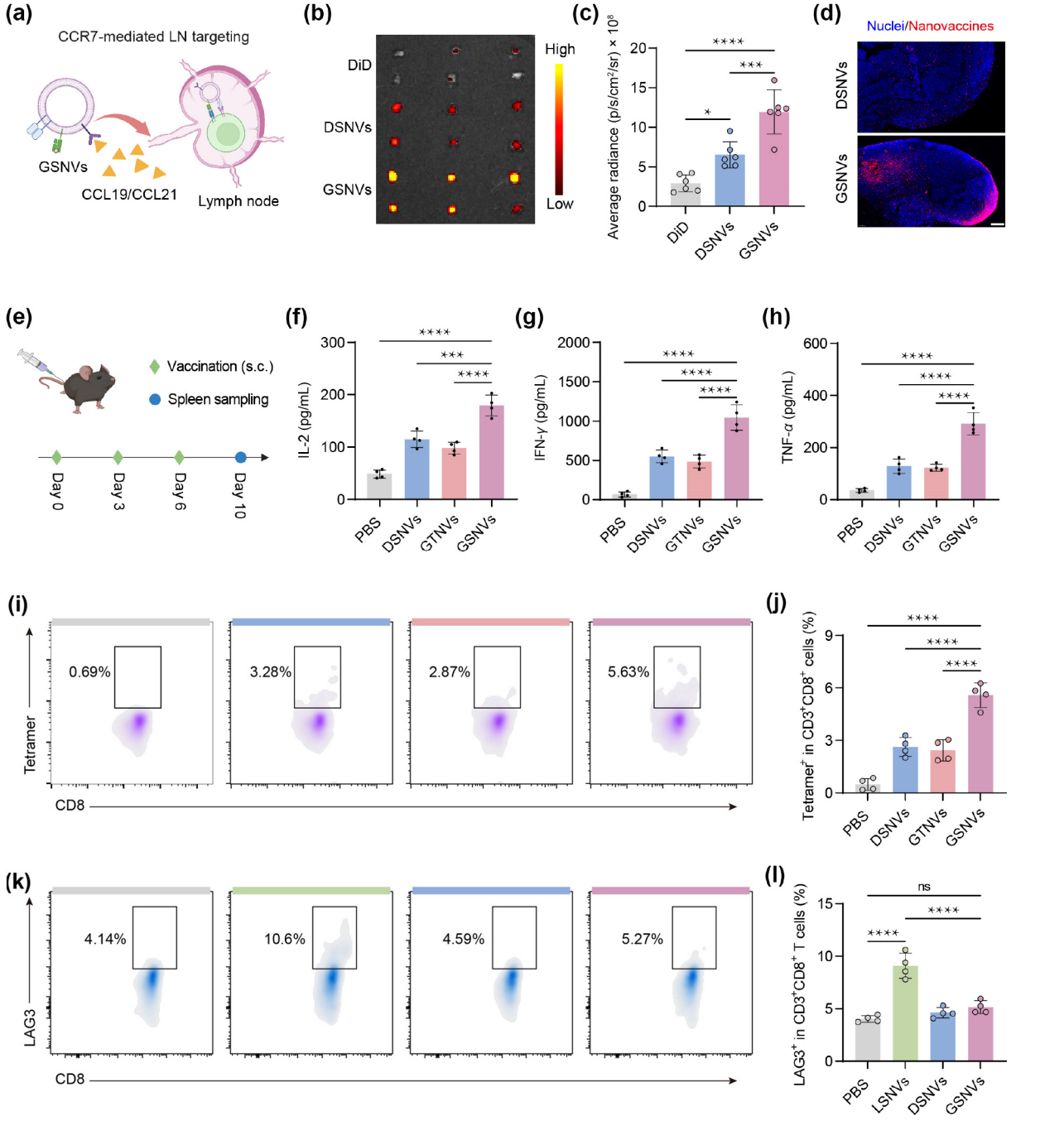

Figure 5 GSNVs exhibited enhanced LN trafficking and potent immunostimulatory effects *in vivo*. (a) Schematic illustration of GSNVs migration from the injection site to dLNs. (b) Representative IVIS images showing the biodistribution of DiD-labeled GSNVs, DSNVs, and free DiD dye in inguinal LNs 24 h post subcutaneous injection. (c) Quantitative analysis of fluorescence intensity of DiD in dLNs (n = 6). (d) Fluorescence microscopy images of LN sections. Scale bar: 100 μm. (e) Schematic of the immunization schedule for evaluating the *in vivo* immune responses. Cytokine levels ((f) IL-2, (g) IFN-γ, and (h) TNF-α) secreted by antigen-repulsed splenocytes derived from immunized mice (n = 4). (i) Representative flow cytometric plots and (j) quantitative analysis of SIINFEKL-tetramer$^+$ CD8$^+$ T cells in spleens (n = 4). (k) Representative flow cytometric plots and (l) quantitative analysis of LAG3$^+$CD8$^+$ T cells in spleens (n = 4). Data are presented as mean ± SD. *P < 0.05, ***P < 0.001, ****P < 0.0001.

efficacy was lower than that of GSNVs. To further investigate the underlying mechanism, we analyzed exhaustion markers (TIM-3 and PD-1) on tumor-infiltrating CD8$^+$ T cells by flow cytometry [51]. Although LSNVs demonstrated notable antitumor activity, the elevated PD-L1 may induce CD8$^+$ T cell exhaustion (Fig. S15(b) in the ESM), thereby limiting sustained antitumor immune responses. In contrast, GSNVs did not induce T cell exhaustion and effectively elicited durable antitumor immunity, resulting in stronger suppression of tumor growth.

4 Conclusions

In summary, we constructed a ManNAc-engineered DC nanovaccine that effectively overcomes key limitations of conventional DC vaccines, including insufficient LN homing,

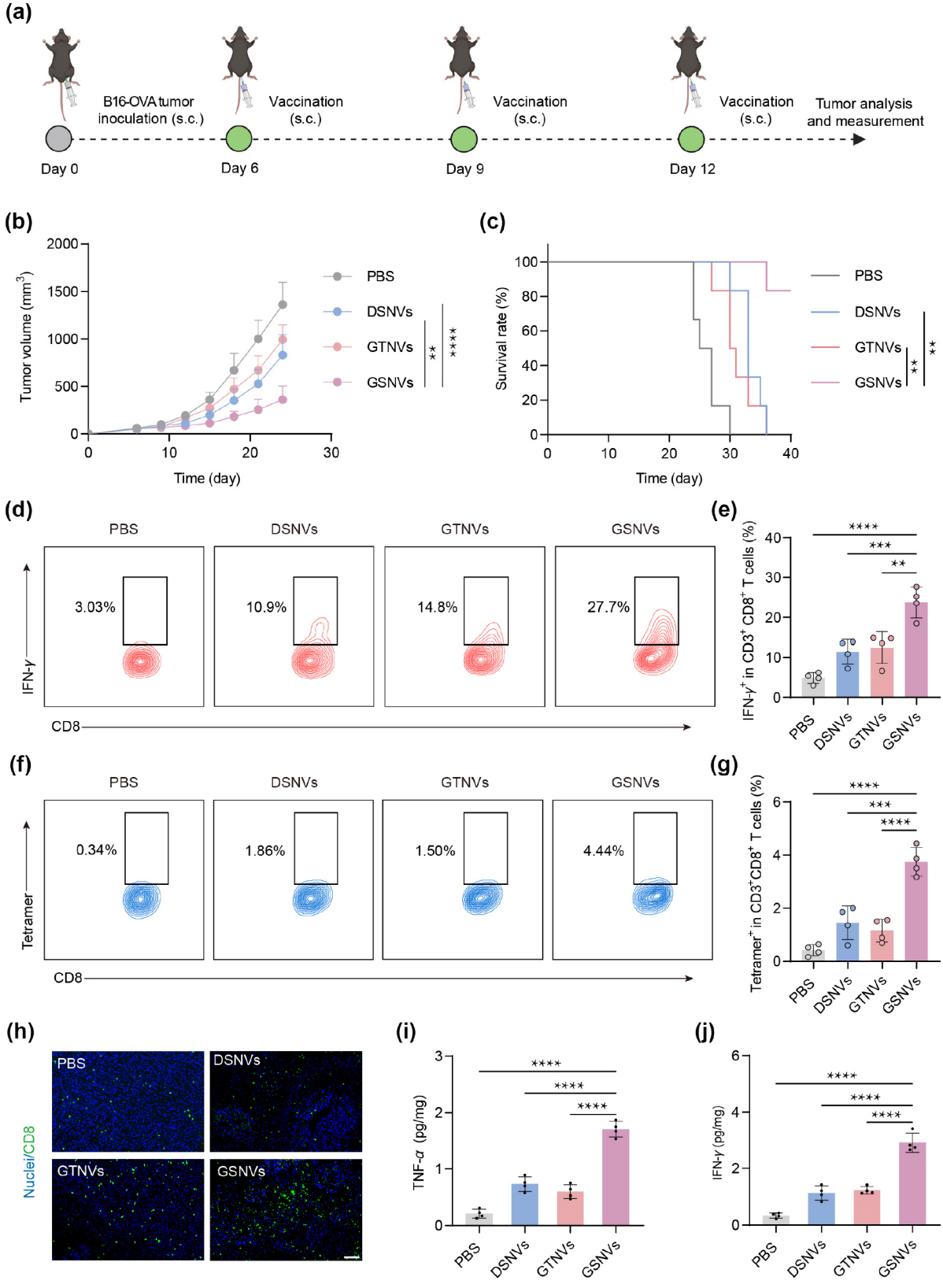

Figure 6 GSNVs elicited robust antitumor immunity in B16-OVA tumor-bearing mice. (a) The therapeutic schedule for B16-OVA-bearing C57BL/6 mice. (b) Average tumor growth curves after treatment with PBS, DSNVs, GTNVs or GSNVs (n = 6). (c) Survival profiles of B16-OVA-bearing C57BL/6 mice receiving different treatments (n = 6). (d) Flow cytometric analysis and (e) quantitative analysis of tumor-infiltrating of IFN-γ^+CD8$^+$ T cells (n = 4). (f) Flow cytometric analysis and (g) quantitative analysis of SIINFEKL-tetramer$^+$ CD8$^+$ T cells within tumors (n = 4). (h) Immunofluorescence staining images showing CD8$^+$ T cell accumulation within tumors. Scale bar: 100 μm. Quantification of proinflammatory cytokines (i) TNF-α and (j) IFN-γ in tumor tissues via ELISA (n = 4). Data are presented as mean ± SD. $^{**}P < 0.01$, $^{***}P < 0.001$, $^{****}P < 0.0001$.

restricted antigen presentation, and suboptimal T cell activation. Following ManNAc engineering, the nanovesicles exhibited increased expression of antigen-MHC-I complexes, co-stimulatory molecules and CCR7 protein, collectively enhancing antigen cross-presentation and promoting efficient migration to LNs. Notably, these engineered GSNVs also showed reduced PD-L1 levels, thereby diminishing immune checkpoint-mediated suppression and facilitating stronger $CD8^+$ T cell activation while alleviating T cell exhaustion. When applied in B16-OVA-bearing mice, GSNVs elicited a potent antigen-specific antitumor immune response, as evidenced by increased infiltration of functional $CD8^+$ T cells (IFN-γ^+ and SIINFEKL-specific $CD8^+$ T cells) and elevated intratumoral levels of IFN-γ and TNF-α. As a result, tumor progression was significantly inhibited and survival was markedly prolonged, demonstrating the potent antitumor efficacy of this vaccine platform. Overall, this strategy offers a promising platform for optimizing DC vaccines and opens new avenues for the design of efficient and personalized vaccines for cancer immunotherapy.

Electronic Supplementary Material: Supplementary material (representative flow cytometric histograms, *in vitro* stability of GSNVs, TEM images and zeta potentials of GTNVs and LSNVs, ELISA analysis of IFN-γ and TNF-α secretion, *in vivo* safety evaluation and antitumor efficacy studies) is available in the online version of this article at https://doi.org/10.26599/NR.2026.94908652.

Data availability

All data needed to support the conclusions in the paper are presented in the manuscript and the Electronic Supplementary Material. Additional data related to this paper may be requested from the corresponding author upon request.

Acknowledgements

This research was supported by the National Natural Science Foundation of China (Nos. 82273874 and 82404561), Liaoning Province Applied Basic Research Program (No. 2025JH2/101330178), Liaoning Revitalization Talents Program (No. XLYC22202019), and Prospective Basic research project of 2024 Scientific Research Project of Liaoning Department of Education (No. LJ212410163042). We also acknowledge app.Biorender.com for assistance in creating the illustration figures.

Declaration of competing interest

All the contributing authors report no conflict of interests in this work.

Author contribution statement

X. Y. F.: Conceptualization, original draft, methodology, investigation. F. X. L.: Methodology, investigation. X. W. J.: Methodology, investigation. L. L. D.: Methodology. Z. G. H.: Investigation. S. J. W.: Conceptualization, review & editing. J. S.: Conceptualization, review & editing, funding acquisition. K. Y. W.: Conceptualization, review & editing, funding acquisition.

Informed consent

Not applicable.

Ethics statement

All the animals were obtained from the Laboratory Animal Center of Shenyang Pharmaceutical University (Shenyang, Liaoning, China). All the animal experiments were approved by the Institutional Animal Care and Use Committee (IACUC) of Shenyang Pharmaceutical University (ethics code: SYPU-IACUC-2025-0302-098).

Use of AI statement

None.

References

[1] Littman, D. R. Releasing the brakes on cancer immunotherapy. *Cell* **2015**, *162*, 1186–1190.

[2] Kraehenbuehl, L.; Weng, C. H.; Eghbali, S.; Wolchok, J. D.; Merghoub, T. Enhancing immunotherapy in cancer by targeting emerging immunomodulatory pathways. *Nat. Rev. Clin. Oncol.* **2022**, *19*, 37–50.

[3] Antonarelli, G.; Corti, C.; Tarantino, P.; Ascione, L.; Cortes, J.; Romero, P.; Mittendorf, E. A.; Disis, M. L.; Curigliano, G. Therapeutic cancer vaccines revamping: Technology advancements and pitfalls. *Ann. Oncol.* **2021**, *32*, 1537–1551.

[4] Fan, X. Y.; Wang, K. Y.; Lu, Q.; Lu, Y. T.; Sun, J. Cell-based drug delivery systems participate in the cancer immunity cycle for improved cancer immunotherapy. *Small* **2023**, *19*, 2205166.

[5] Saxena, M.; Van Der Burg, S. H.; Melief, C. J. M.; Bhardwaj, N. Therapeutic cancer vaccines. *Nat. Rev. Cancer* **2021**, *21*, 360–378.

[6] Li, Y.; Tong, F.; Wang, Y. F.; Wang, J.; Wu, M. Q.; Li, H. M.; Guo, H. Y.; Gao, H. L. *In situ* tumor vaccine with optimized nanoadjuvants and lymph node targeting capacity to treat ovarian cancer and metastases. *Acta Pharm. Sin. B* **2024**, *14*, 4102–4117.

[7] Meng, J. Q.; Lv, Y. L.; Bao, W. E.; Meng, Z. H.; Wang, S.; Wu, Y. B.; Li, S. P.; Jiao, Z. G.; Tian, Z. Y.; Ma, G. H. et al. Generation of whole tumor cell vaccine for on-demand manipulation of immune responses against cancer under near-infrared laser irradiation. *Nat. Commun.* **2023**, *14*, 4505.

[8] Li, Q.; Zeng, H.; Liu, T.; Wang, P. P.; Zhang, R.; Zhao, B. Y.; Feng, T.; Yang, Y. L.; Wu, J. M.; Zheng, Y. et al. A dendritic cell vaccine for both vaccination and neoantigen-reactive T cell preparation for cancer immunotherapy in mice. *Nat. Commun.* **2024**, *15*, 10419.

[9] He, X. L.; Du, J.; Zeng, L. Z.; Tong, F.; Ma, J. Q.; Zeng, N.; Hu, C.; Gao, H. L.; Zhang, J. M. Advances in nanotechnology-augmented T cell-based novel cancer immunotherapies. *Nano Res.* **2026**, *19*, 94908299.

[10] Heras-Murillo, I.; Adán-Barrientos, I.; Galán, M.; Wculek, S. K.; Sancho, D. Dendritic cells as orchestrators of anticancer immunity and immunotherapy. *Nat. Rev. Clin. Oncol.* **2024**, *21*, 257–277.

[11] Steinman, R. M. Decisions about dendritic cells: Past, present, and future. *Ann. Rev. Immunol.* **2012**, *30*, 1–22.

[12] Yang, H.; Xiong, Z. J.; Heng, X. Y.; Niu, X. M.; Wang, Y. C.; Yao, L. H.; Sun, L. L.; Liu, Z.; Chen, H. Click-chemistry-mediated cell membrane glycopolymer engineering to potentiate dendritic cell vaccines. *Angew. Chem., Int. Ed.* **2024**, *63*, e202315782.

[13] Steinman, R. M.; Banchereau, J. Taking dendritic cells into medicine. *Nature* **2007**, *449*, 419–426.

[14] Palucka, K.; Banchereau, J. Cancer immunotherapy via dendritic cells. *Nat. Rev. Cancer* **2012**, *12*, 265–277.

[15] Mahadevan, K. K.; Dyevoich, A. M.; Chen, Y.; Li, B. R.; Sugimoto, H.; Sockwell, A. M.; McAndrews, K. M.; Sthanam, L. K.; Wang, H.

M.; Shalapour, S. et al. Type I conventional dendritic cells facilitate immunotherapy in pancreatic cancer. *Science* **2024**, *384*, eadh4567.

[16] Fløisand, Y.; Remberger, M.; Bigalke, I.; Josefsen, D.; Vålerhaugen, H.; Inderberg, E. M.; Olaussen, R. W.; Gjertsen, B. T.; Goedkoop, R.; Geiger, C. et al. WT1 and PRAME RNA-loaded dendritic cell vaccine as maintenance therapy in de novo AML after intensive induction chemotherapy. *Leukemia* **2023**, *37*, 1842–1849.

[17] Sabado, R. L.; Balan, S.; Bhardwaj, N. Dendritic cell-based immunotherapy. *Cell Res.* **2017**, *27*, 74–95.

[18] Santana-Magal, N.; Farhat-Younis, L.; Gutwillig, A.; Gleiberman, A.; Rasoulouniriana, D.; Tal, L.; Netanely, D.; Shamir, R.; Blau, R.; Feinmesser, M. et al. Melanoma-secreted lysosomes trigger monocyte-derived dendritic cell apoptosis and limit cancer immunotherapy. *Cancer Res.* **2020**, *80*, 1942–1956.

[19] Lu, Y. C.; Shi, Y. Y.; Liu, Y.; Luo, Z. Y.; Zhang, J. L.; Jiang, M. S.; Li, X.; Liu, X.; Guo, X. M.; Qin, B. et al. A therapeutic DC vaccine with maintained immunological activity exhibits robust anti-tumor efficacy. *J. Control. Release* **2022**, *349*, 254–268.

[20] Park, D.; Lapteva, N.; Seethammagari, M.; Slawin, K. M.; Spencer, D. M. An essential role for Akt1 in dendritic cell function and tumor immunotherapy. *Nat. Biotechnol.* **2006**, *24*, 1581–1590.

[21] Joffre, O. P.; Segura, E.; Savina, A.; Amigorena, S. Cross-presentation by dendritic cells. *Nat. Rev. Immunol.* **2012**, *12*, 557–569.

[22] Sun, L. L.; Shen, F. Y.; Xiong, Z. J.; Yang, H.; Dong, Z. L.; Xiang, J.; Gu, Q. Y.; Ji, Q. S.; Fan, C. H.; Liu, Z. DNA engineered lymphocyte-based homologous targeting artificial antigen-presenting cells for personalized cancer immunotherapy. *J. Am. Chem. Soc.* **2022**, *144*, 7634–7645.

[23] Oh, S. A.; Wu, D. C.; Cheung, J.; Navarro, A.; Xiong, H. Z.; Cubas, R.; Totpal, K.; Chiu, H.; Wu, Y.; Comps-Agrar, L. et al. PD-L1 expression by dendritic cells is a key regulator of T-cell immunity in cancer. *Nat. Cancer* **2020**, *1*, 681–691.

[24] Xu, Y. T.; Zhu, W. X.; Wu, J. C.; Liu, L. J.; Yue, L. D.; Zhang, X. Y.; Li, J. Y.; She, P.; Yang, J. J.; Sun, C. L. et al. 3D-printed dendritic cell vaccines for post-surgery cancer immunotherapy. *Adv. Funct. Mater.* **2024**, *34*, 2400507.

[25] Yi, W. Z.; Qian, X. D.; Yan, D.; Yan, W. L.; Hu, S. S.; Li, Y. P.; Wang, D. G. A dendritic cell-nanogel conjugate for tumor-draining lymph node-specific PD-L1 blockade. *Adv. Mater.* **2025**, *37*, 2504733.

[26] Mayoux, M.; Roller, A.; Pulko, V.; Sammicheli, S.; Chen, S.; Sum, E.; Jost, C.; Fransen, M. F.; Buser, R. B.; Kowanetz, M. et al. Dendritic cells dictate responses to PD-L1 blockade cancer immunotherapy. *Sci. Trans. Med.* **2020**, *12*, eaav7431.

[27] Sharma, P.; Goswami, S.; Raychaudhuri, D.; Siddiqui, B. A.; Singh, P.; Nagarajan, A.; Liu, J. L.; Subudhi, S. K.; Poon, C.; Gant, K. L. et al. Immune checkpoint therapy-current perspectives and future directions. *Cell* **2023**, *186*, 1652–1669.

[28] Roerden, M.; Spranger, S. Cancer immune evasion, immunoediting and intratumour heterogeneity. *Nat. Rev. Immunol.* **2025**, *25*, 353–369.

[29] Wu, F. H.; Guo, Z. F.; Yang, J. L.; Ou, Y. S.; Xie, X. J.; Liao, H.; Guo, C. Q.; Zhan, Y. X.; Wu, H. P.; Hu, R. et al. A universal therapeutic vaccine leveraging autologous pre-existing immunity to eliminate *in situ* uniformly engineered heterogeneous tumor cells. *Adv. Mater.* **2025**, *37*, 2412430.

[30] Khleif, S. N.; Gupta, S. Cancer vaccines as enablers of immunotherapy. *Nat. Immunol.* **2025**, *26*, 1877–1889.

[31] Rao, L.; Yuan, Y.; Shen, X.; Yu, G. C.; Chen, X. Y. Designing nanotheranostics with machine learning. *Nat. Nanotechnol.* **2024**, *19*, 1769–1781.

[32] Zhao, C. C.; Pan, Y. W.; Cao, L.; Tang, Y. J.; Chen, X. Y.; Zhao, X. Z.; Rao, L. Metal-phenolic outer membrane vesicles for cancer radioimmunotherapy. *J. Am. Chem. Soc.* **2025**, *147*, 26195–26207.

[33] You, Q.; Wu, G. G.; Li, H.; Liu, J. Y.; Cao, F. F.; Ding, L. W.; Liang, F. M.; Zhou, B.; Ma, L. L. S.; Zhu, L. et al. A nanovaccine targeting cancer stem cells and bulk cancer cells for postoperative cancer immunotherapy. *Nat. Nanotechnol.* **2025**, *20*, 1298–1311.

[34] Lin, X. Y.; Yue, L. D.; Cheng, K.; Rao, L. Engineering cellular vesicles for immunotherapy. *Acc. Mater. Res.* **2025**, *6*, 327–339.

[35] Feng, K. H.; Zhang, X. R.; Li, J. L.; Han, M. Z.; Wang, J. H.; Chen, F. C.; Yi, Z. W.; Di, L. Q.; Wang, R. N. Neoantigens combined with *in situ* cancer vaccination induce personalized immunity and reshape the tumor microenvironment. *Nat. Commun.* **2025**, *16*, 5074.

[36] Liu, C.; Liu, X.; Xiang, X. C.; Pang, X.; Chen, S. Y.; Zhang, Y. M.; Ren, E.; Zhang, L. L.; Liu, X.; Lv, P. et al. A nanovaccine for antigen self-presentation and immunosuppression reversal as a personalized cancer immunotherapy strategy. *Nat. Nanotechnol.* **2022**, *17*, 531–540.

[37] Wu, K. R.; Lyu, F.; Wu, S. Y.; Sharma, S.; Deshpande, R. P.; Tyagi, A.; Zhao, D.; Xing, F.; Singh, R.; Watabe, K. Engineering an active immunotherapy for personalized cancer treatment and prevention of recurrence. *Sci. Adv.* **2023**, *9*, eade0625.

[38] Wang, K. Y.; Zhang, X. B.; Ye, H.; Wang, X.; Fan, Z. J.; Lu, Q.; Li, S. H.; Zhao, J.; Zheng, S. Z.; He, Z. G. et al. Biomimetic nanovaccine-mediated multivalent IL-15 self-transpresentation (MIST) for potent and safe cancer immunotherapy. *Nat. Commun.* **2023**, *14*, 6748.

[39] Yang, C.; Chen, Y. L.; Liu, J.; Zhang, W. S.; He, Y.; Chen, F. M.; Xie, X. C.; Tang, J.; Guan, S.; Shao, D. et al. Leveraging senescent cancer cell membrane to potentiate cancer immunotherapy through biomimetic nanovaccine. *Adv. Sci.* **2024**, *11*, 2400630.

[40] Nguyen, N. T.; Le, X. T.; Lee, W. T.; Lim, Y. T.; Oh, K. T.; Lee, E. S.; Choi, H. G.; Youn, Y. S. STING-activating dendritic cell-targeted nanovaccines that evoke potent antigen cross-presentation for cancer immunotherapy. *Bioact. Mater.* **2024**, *42*, 345–365.

[41] Zhang, J.; Fan, B.; Cao, G. L.; Huang, W. P.; Jia, F. H.; Nie, G. J.; Wang, H. Direct presentation of tumor-associated antigens to induce adaptive immunity by personalized dendritic cell-mimicking nanovaccines. *Adv. Mater.* **2022**, *34*, 2205950.

[42] Lu, J. Y.; Miao, F. Z.; Zhao, Y. C.; Liu, J.; Meng, Y.; Yan, H.; Wang, R. Y.; Zhu, Q. G.; Tai, Z. G.; Chen, Z. J. Biomimetic nanovesicle vaccines derived from dendritic cells sensitized with whole tumor antigens for melanoma immunotherapy. *Mater. Today Bio* **2025**, *35*, 102409.

[43] Marin, I.; Boix, O.; Garcia-Garijo, A.; Sirois, I.; Caballe, A.; Zarzuela, E.; Ruano, I.; Attolini, C. S. O.; Prats, N.; López-Domínguez, J. A. et al. Cellular senescence is immunogenic and promotes antitumor immunity. *Cancer Discov.* **2023**, *13*, 410–431.

[44] Hong, J.; Jung, M.; Kim, C.; Kang, M.; Go, S.; Sohn, H.; Moon, S.; Kwon, S.; Song, S. Y.; Kim, B. S. Senescent cancer cell-derived nanovesicle as a personalized therapeutic cancer vaccine. *Exp. Mol. Med.* **2023**, *55*, 541–554.

[45] Han, J.; Bhatta, R.; Liu, Y. S.; Bo, Y.; Elosegui-Artola, A.; Wang, H. Metabolic glycan labeling immobilizes dendritic cell membrane and enhances antitumor efficacy of dendritic cell vaccine. *Nat. Commun.* **2023**, *14*, 5049.

[46] Förster, R.; Davalos-Misslitz, A. C.; Rot, A. CCR7 and its ligands: Balancing immunity and tolerance. *Nat. Rev. Immunol.* **2008**, *8*, 362–371.

[47] Xia, Y. M.; Fu, S. L.; Ma, Q. P.; Liu, Y. J.; Zhang, N. Application of nano-delivery systems in lymph nodes for tumor immunotherapy. *Nano-Micro Lett.* **2023**, *15*, 145.

[48] Miao, Y.; Niu, L.; Lv, X. Y.; Zhang, Q.; Xiao, Z. S.; Ji, Z. X.; Chen, L. F.; Liu, Y.; Liu, N. H.; Zhu, J. J. et al. A minimalist pathogen-like sugar nanovaccine for enhanced cancer immunotherapy. *Adv. Mater.* **2024**, *36*, 2410715.

[49] Li, N.; Qin, H.; Zhu, F.; Ding, H.; Chen, Y.; Lin, Y. X.; Deng, R. H.; Ma, T. Y.; Lv, Y. Y.; Xiong, C. H. et al. Potent prophylactic cancer vaccines harnessing surface antigens shared by tumour cells and induced pluripotent stem cells. *Nat. Biomed. Eng.* **2025**, *9*, 215–233.

[50] Pan, X. T.; Wang, Z. H.; Tan, M. X.; Fu, Z. Y.; Nie, G. J.; Wang, H. Nanoinducer-mediated mitochondria-selective degradation enhances T cell immunotherapy against multiple cancers. *Nat. Nanotechnol.* **2025**, *20*, 947–958.

[51] Zhang, Z. Y.; Ren, C. Y.; Xiao, R.; Ma, S. Y.; Liu, H. M.; Dou, Y. T.; Fan, Y. C.; Wang, S.; Zhan, P.; Gao, C. J. et al. Palmitoylation of TIM-3 promotes immune exhaustion and restrains antitumor immunity. *Sci. Immunol.* **2024**, *9*, eadp7302.